NANO LETTERS

pubs.acs.org/NanoLett Letter

Nonadiabatic Dynamics of Photocatalytic Water Splitting on A Polymeric Semiconductor

Peiwei You, Chao Lian, Daqiang Chen, Jiyu Xu, Cui Zhang,* Sheng Meng,* and Enge Wang*

Cite This: *Nano Lett.* 2021, 21, 6449−6455 Read Online

ACCESS | Metrics & More | Article Recommendations | Supporting Information

ABSTRACT: To elucidate the nature of light-driven photocatalytic water splitting, a polymeric semiconductor—graphitic carbon nitride ($g\text{-}C_3N_4$)—has been chosen as a prototype substrate for studying atomistic water spitting processes in realistic environments. Our nonadiabatic quantum dynamics simulations based on real-time time-dependent density functional theory reveal explicitly the transport channel of photogenerated charge carriers at the $g\text{-}C_3N_4$/water interface, which shows a strong correlation to bond re-forming. A three-step photoreaction mechanism is proposed, whereas the key roles of hole-driven hydrogen transfer and interfacial water configurations were identified. Immediately following photocatalytic water splitting, atomic pathways for the two dissociated hydrogen atoms approaching each other and forming the H_2 gas molecule are demonstrated, while the remanent OH radicals may form intermediate products (e.g., H_2O_2). These results provide critical new insights for the characterization and further development of efficient water-splitting photocatalysts from a dynamic perspective.

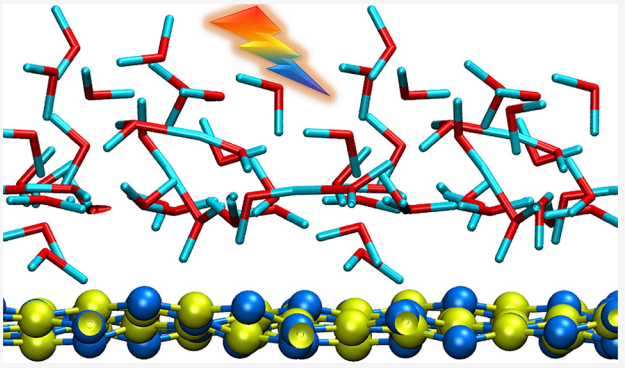

KEYWORDS: *ab initio calculations, photocatalysis, graphitic carbon nitride, bond evolution, time dependent density functional theory*

Owing to its high chemical stability, suitable bandgap, and "earth-abundant" nontoxic nature, graphitic carbon nitride ($g\text{-}C_3N_4$), a polymeric visible-light-active semiconductor photocatalyst, has received tremendous attentions for utilization in efficient solar water splitting[1−4] and other catalytic synthesis.[5−7] Functionalizing $g\text{-}C_3N_4$ photocatalyst via embedding metal atoms, carbon dots, and sulfur dopants can further improve its performance and attain more active sites, better optical and electronic properties, and higher efficiency for both hydrogen and oxygen evolutions.[8−11] By tuning the synthesis conditions, the morphology of $g\text{-}C_3N_4$ could be adjusted to obtain large surface areas and impressing optical performance.[12−14] One can also combine $g\text{-}C_3N_4$ with other two-dimensional materials, such as black phosphorus,[15] molybdenum disulfide[16,17] and graphene,[18,19] to achieve enhanced photoactivity. For example, fabrication of a carbon nanodots−C_3N_4 nanocomposite remarkably boosts its performance of photocatalytic water splitting by a two-step pathway under visible light, where $g\text{-}C_3N_4$ is responsible for the first photocatalytic step and carbon dots account for the secondary chemical synthesis step.[11] Recent synchronous X-ray photoelectron spectroscopy measurements have revealed the electron transfer and bond evolution pathways in Pt-decorated $g\text{-}C_3N_4$ catalyst under light irradiation.[20]

Although significant progress has been made in the photocatalytic applications of $g\text{-}C_3N_4$ materials for water splitting, description of the underlying fundamental steps and understanding atomistic mechanisms are far from complete. For instance, the precise atomic sites for splitting the OH bonds are unknown and whether electron or hole transfer drives the processes remains ambiguous. Theoretical models and computational studies offer a powerful tool to investigate the principles of photocatalytic water splitting reactions and complement the experiments. As a schematic model, adsorption of a single water molecule on $g\text{-}C_3N_4$ sheet was previously explored by first-principles approaches.[21−23] The studies reported that the buckled sheet, rather than the planar $g\text{-}C_3N_4$, is more favorable for water adsorption and the most stable adsorption configuration comprises a water molecule standing on top of the intrinsic vacancy with an adsorption energy of ∼0.5 eV. However, the simple models with one to a few water molecules neglect the complex solid−liquid interactions and the intertwined structural and electronic properties of water/$g\text{-}C_3N_4$ interface under real circumstances for solar-to-hydrogen production.[24] In addition, photocatalytic water splitting on $g\text{-}C_3N_4$ involves rapid charge transfer between the catalyst and the liquid, a nonadiabatic excited state phenomenon where motions of electrons and nuclei are

Received: March 24, 2021
Revised: July 10, 2021
Published: July 19, 2021

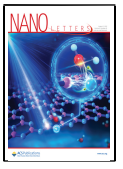

https://doi.org/10.1021/acs.nanolett.1c01187
Nano Lett. 2021, 21, 6449−6455

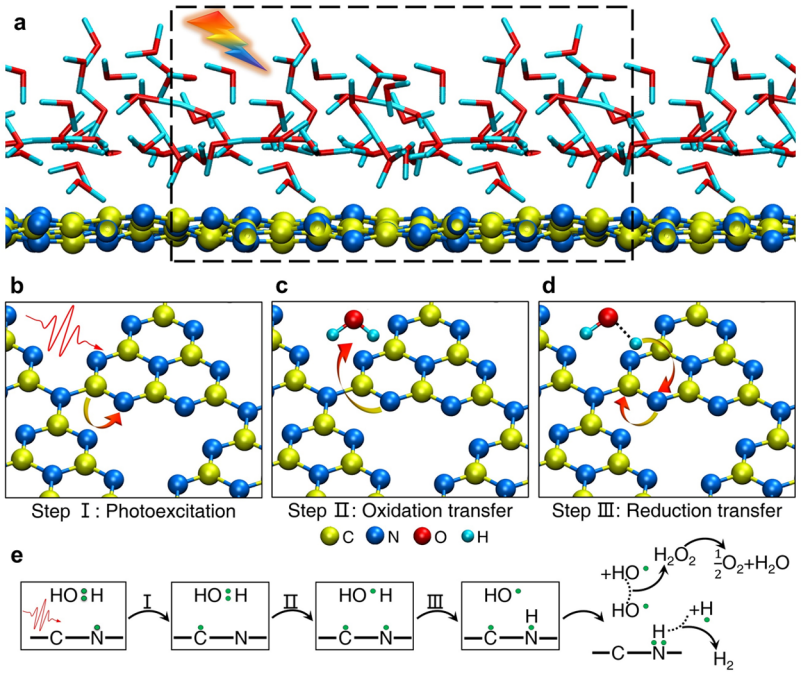

Figure 1. (a) Atomic configuration of the g-C_3N_4 /water interface in the simulation supercell and its periodic images. (b–d) Schematic diagrams of three-step photocatalytic water splitting processes on g-C_3N_4. The arrows indicate the direction of hole/H^+ current. (e) General scheme for entangled electron-nuclei mechanism in the three-step model, where green dots denote typical electrons. Possible formations of hydrogen peroxide, oxygen gas, and hydrogen gas are also displayed.

strongly coupled. Traditional Born–Oppenheimer approximation, wherein the electrons and nuclei are decoupled, breaks down. Therefore, to probe the time-domain propagation of excited states, an effective first-principles approach for nonadiabatic molecular dynamics (MD), such as that formulated within the real-time time-dependent density functional theory (rt-TDDFT) framework,[25−31] is strongly desired. Recent works on light-induced water splitting focus on field enhancement effects near the surface of nanomaterials, caused by too strong laser field (up to ∼9 V/Å), far from realistic situations.[32,33] Moreover, the crucial effects of photogenerated electron–hole pairs were completely ignored. The photoinduced proton transfer between a heptazine molecule and small water clusters has been studied using surface hopping simulations;[34] however, it is limited to finite molecular systems in the absence of light field, which are quite different from real situations of photosplitting at the liquid water/semiconductor interface.

In this work, we employ *ab initio* rt-TDDFT molecular dynamics simulations to investigate the atomistic steps and fundamental mechanisms of photocatalytic reactions at g-C_3N_4/water interface (Figure 1). Nonadiabatic MD simulations allow us to identify the crucial photoinduced electron excitation and transfer processes, and unravel the pathways of photogenerated charge carriers to drive the reactions. We propose a three-step reaction mechanism for the photoinduced water splitting on g-C_3N_4 upon light irradiation, comprising photoexcitation (Figure 1b), oxidation transfer (Figure 1c), and reduction transfer (Figure 1d) processes. We identify the hydrogen transfer reaction in g-C_3N_4 photocatalysis to be hole-driven, and we establish the corresponding relationship between charge transfer and bond re-forming. Furthermore, the hydrogen gas molecule can be formed via the aggregation of two split hydrogen atoms near the reaction center of g-C_3N_4.

We apply the laser pulse with a Gaussian envelope as shown in Figure 2a, where the maximum intensity is 0.1 V/Å. The laser peak intensity is 5.6×10^{11} (W/cm^2), which is indeed stronger than the solar irradiation intensity but can be readily

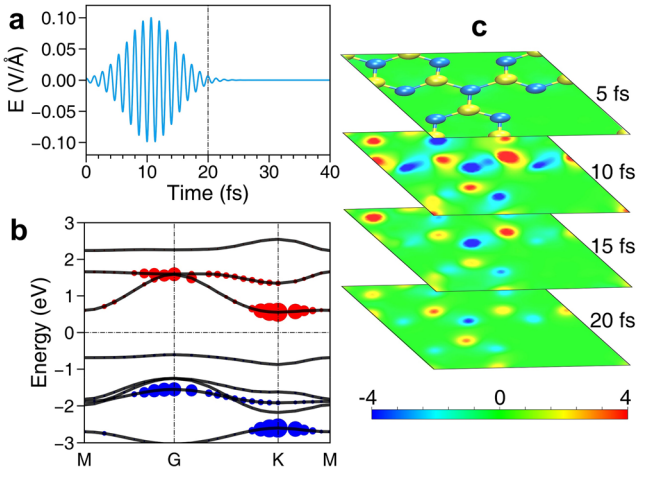

Figure 2. (a) Time evolution waveform of the laser field $E(t) = E_{max}\cos(\omega t)\exp\left[-\frac{(t-t_0)^2}{2\sigma^2}\right]$, where the photon energy $\hbar\omega$ = 3.1 eV, the maximum field intensity E_{max} = 0.1 V/Å, and the time to peak t_0 = 12.5 fs. (b) Excited band structure of g-C_3N_4 upon laser irradiation extracted from the rt-TDDFT MD simulation at 20 fs. The size of red and blue dots indicates the population of excited electrons and holes generated by the laser pulse. (c) Electron density differences between the photoinduced excited state and the initial ground state for g-C_3N_4 under laser action at 5, 10, 15, and 20 fs, respectively, where the unit of electron density is 10^{-3} e/Bohr^3.

https://doi.org/10.1021/acs.nanolett.1c01187
Nano Lett. 2021, 21, 6449−6455

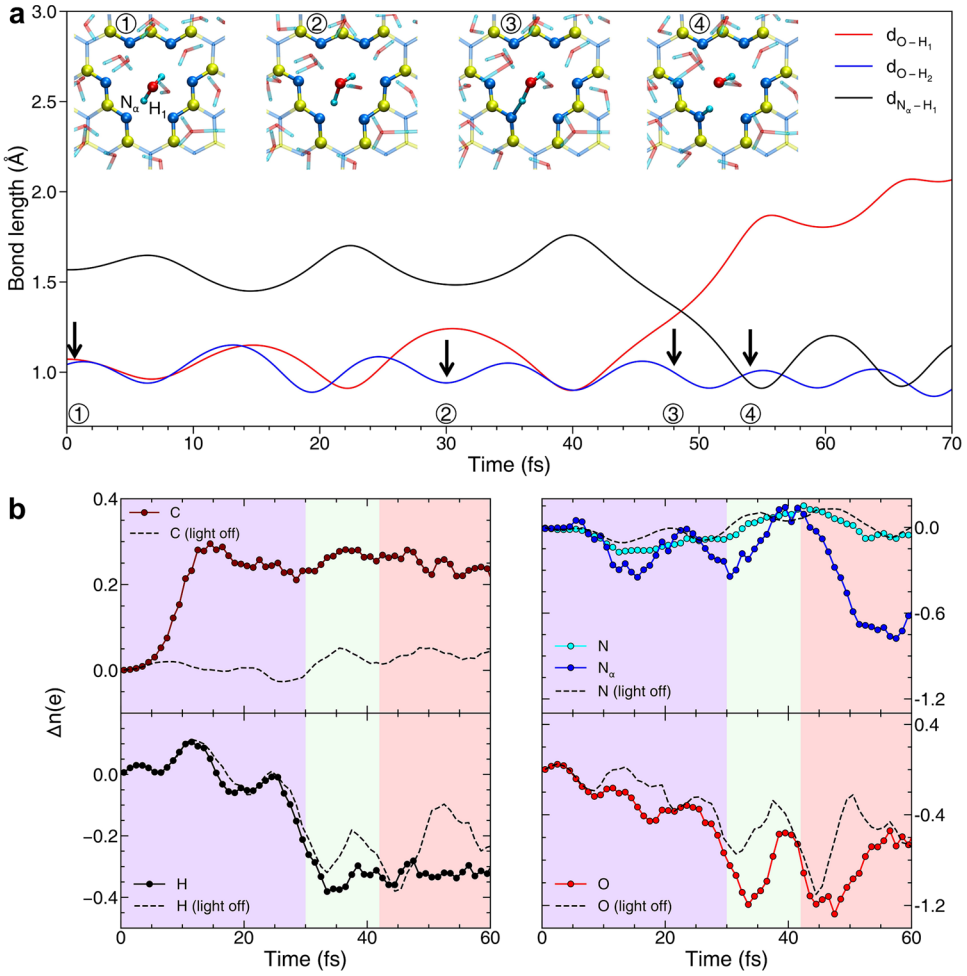

Figure 3. (a) Time evolution of the O−H and N_α-H_1 distances for the splitting water molecule. Snapshots at four representative times (0, 30, 48, and 54 fs) during the photocatalytic water splitting process on g-C_3N_4 are shown in the insets ①−④. N_α denotes the nitrogen atom on g-C_3N_4 that adsorbs hydrogen at the end of photoreaction. (b) Time evolution of electron populations for the atoms at the reaction center (highlighted in the insets) in the period of 0−30 fs (photoexcitation, violet span), 30−42 fs (oxidation transfer, green span), and 42−60 fs (reduction transfer, red span), respectively. Dashed lines denote the control group without light.

achieved in laser experiment. The injected energy fluence is 2.0 (mJ/cm^2) in the duration of 30 fs, which is much smaller than the injected energy 122.7 (J/cm^2) during 12 h mimetic solar irradiation in experiments.[11] Although the photocarrier relaxation processes and the overall energy conversion efficiency might be different, our simulation still captures the quantum water splitting nature in solar light since one photon can only excite one electron−hole pair in these regimes. Thus, this laser field can be considered as a collection of multiple photons acting in a short period in the visible light region. Since the ultrafast photon−membrane interaction time is short ($\sim 1 \times 10^{-9}$ m/3 × 10^8 m/s ≈ 10^{-18} s) and a typical energy per solar photon is 2.5 eV, a field strength of 2.5 eV/10^{-18} s per area of g-C_3N_4 sheet ≈10^{13} W/cm^2 is also relevant for the quantum nature of water splitting under solar irradiance.

The band structure of photoexcited g-C_3N_4 is displayed in Figure 2b. We chose the photon energy of 3.1 eV for the simulations because it is slightly higher than the experimental band gap of g-C_3N_4 (2.7 eV);[1,9,10] therefore, the charge excitation occurs between energy levels lower than the valence band maximum (lines with blue dots) and the conduction band edge (lines with red dots). The band structure obtained from the PBE and hybrid HSE06 functionals exhibit very similar band features and the position of charge carriers upon irradiation is almost the same (Figure S1). We also check our results by adopting an energy scissor correction of 1.4 eV to shift energy levels of the conduction band, and empirically correct the calculated band gap of g-C_3N_4 to ∼2.7 eV, as shown in Figure S2. The photoexcitation processes initiated by 3.1 eV photon in the original case and 4.5 eV photon on the gap-corrected system yield very similar results, which are both attributed to the strong dipolar transitions between the deep valence band (N 2p orbits) and the conduction band minimum.

The photoexcited electrons in g-C_3N_4 are transferred from the N 2p orbitals in the valence band to the C 2p orbitals in the conduction band. These changes can be localized in real-space. In Figure 2c, we display the electron density difference of the photoinduced excited state of g-C_3N_4, with respect to its initial ground state, at 5, 10, 15, and 20 fs, respectively. It shows that the excited electrons are mainly concentrated around carbon atoms, while the holes are localized near nitrogen atoms after the charge transfer process is activated by the light in g-C_3N_4.

We then investigate the photoinduced dynamics of water at the g-C_3N_4/water interface (More method details in

https://doi.org/10.1021/acs.nanolett.1c01187
Nano Lett. 2021, 21, 6449−6455

Supporting Information). The supercell of g-C_3N_4/water interface consists of a (2 × 2) g-C_3N_4 sheet and 31 water molecules with a density of ∼1 g/cm^2. We first equilibrate the g-C_3N_4/water interface in the constant-energy ensemble (*NVE*) at 300 K using ground-state MD simulations, and then activate the photoexcitation dynamic process at the interface by applying an external light field parallel to the surface (Figure 2a). In our rt-TDDFT MD simulations, the photoinduced water splitting process on g-C_3N_4 is monitored.

In Figure 3a, we present the bond length changes as a function of time for the water molecule which splits during the simulation. The four representative configurations during the reaction are also illustrated. In the time span of light irritation (0−20 fs), we observe that the water molecule (highlighted in the insets) first approaches one of the nitrogen atoms (labeled as N_α) at the perimeter of the intrinsic vacancy of g-C_3N_4 sheet, forming a hydrogen bond with N_α, and then splits in the period of 42−60 fs with a hydrogen atom (H_1) transferring to N_α.

To identify the driving force for such photoinduced water splitting at the g-C_3N_4/water interface, we partition the electron density into each atom by Hirshfeld charge analysis. In Figure 3b, we show the time evolution of averaged electron population on the atoms at the reaction center of g-C_3N_4, as highlighted in the insets of Figure 3a. The initial state of g-C_3N_4/water interface is set as the reference to illustrate the time-dependent changes of electron population.

In the photoexcitation period (0−30 fs) under the direct stimulation of laser pulse, major charge transfer from nitrogen to carbon atoms is found in g-C_3N_4, as shown in the violet span of Figure 3b, where the variations of electron population for nine carbon and six nitrogen atoms are presented as a function of time. The electron population of water molecule remains nearly constant with small oscillations at the end of pulse. Compared to the case without light (dashed lines in Figure 3b), we find that the light is mainly absorbed by the g-C_3N_4 sheet in this photoexcitation stage, yielding an excitation channel for hole transfer from carbon to nitrogen.

After the direct excitation by laser, the entire system evolves in its excited state. During the time span of 30−42 fs, we find a hole transfer (∼0.4 e) from N_α to water molecule, especially to the H atom of the adjacent water molecule (see green span in Figure 3b). The electron density isosurfaces in Figure S3 also display a dynamic shift of electron cloud from H_1 to N_α, revealing the hole transfer process. The time-resolved projected density of states and corresponding orbital occupation in Figure S4 show that the hole on the nitrogen atoms of g-C_3N_4 has disappeared and been transferred to the oxygen orbitals in water near the Fermi level, while the conduction band electrons follow a conventional decay pathway. Such oxidation charge transfer process for water molecule leads to a decrease of OH bond strength and a moderate increment of OH_1 bond oscillation frequency, as shown in Figure 3a, indicating the hole transfer process may affect the vibrational mode of water and result in a vibration excitation.[35]

In the following period between 42−60 fs, we discover a reverse hole injection (∼1.0 e) from the splitting water molecule to N_α on g-C_3N_4, presenting a reduction charge transfer process of water in Figure 3d. The hole transfer from water to N_α leads to the enhancement of hydrogen bonding between N_α in g-C_3N_4 and H_1 in water molecule, as demonstrated in configuration ③ in Figure 3a. Adequate charge transfer eventually results in the transfer of H_1 to N_α at about 54 fs, forming the N−H bond and a neutral hydroxyl radical. The energy difference between the splitting form (H−OH) and an intact H_2O is 0.37 eV, which can be compensated by the overpotential provided by photoexcited hole. At the end of 60 fs, the ionic OH fragment in water has accumulated about 1e hole, as shown in Figure S5, resulting in a neutral particle state. Since the active hydroxyl radical can help to dissociate a neighboring water molecule, the rise of electrons in OH radial in Figure S5 is also contributed by a dissociated H from neighboring H_2O, where the split configurations can be seen in Figure S6. This also indicates that the active OH radical can facilitate a neighboring water molecule to dissociate. The hydroxyl groups left in the aqueous solution could form intermediate photoproducts such as H_2O_2 and oxygen gas in subsequent reactions, while assembling two and more such adsorbed hydrogen atoms under the condition of electron aggregation could lead to the formation of hydrogen gas.

Time-resolved Fourier transform infrared (FTIR) spectroscopy can be used to track the dynamic bond evolution and identify the intermediates in chemical reactions.[20,36] The stretching vibrational mode of N−H bond and O−H bonds shown in Figure S7 are in the range of 3100−3200 and 3300−3400 cm^{-1}, respectively, consistent with experimental infrared spectra measured in ref 20. This evidence confirms the photoinduced formation of N−H bond, arising from the simulated hole transfer mechanism. Here we evaluate the photon-to-electron quantum efficiency to be 3% for laser-induced water splitting, which is higher than the value (0.1% in ref 11) obtained in experiments, implying the injected photons in a short time may accelerate the photoinduced water splitting process.

Summarizing the above phenomena, we propose a three-step model for photoinduced water splitting on g-C_3N_4 as illustrated in Figure 1b−d: (i) the photoexcitation step, where g-C_3N_4 sheet absorbs photons and initiates hole transfer from carbon to nitrogen atoms; (ii) oxidation transfer step, where a hole current flows from nitrogen atom at the intrinsic vacancy of g-C_3N_4 to the water molecule, resulting in a weakened O-H bond; (iii) reduction transfer step, where a reverse hole flow injects from water to nitrogen, leading to water bond breaking and the hydrogen transfer to g-C_3N_4. A schematic description for the global photoreaction cycle based on electron flow is also shown in Figure 1e. Such a three-step water splitting mechanism unravels how the photogenerated charge carrier transfer drives the breaking and re-forming of chemical bonds on the g-C_3N_4 photocatalyst. We note that for longer time process, the hot carrier cooling (e.g., relaxing to the band edge) might be important.[37,38] In the relaxation process, the decay time is in the range of tens to hundreds of picoseconds in experiments;[15] thus, the excited electron−hole pairs would experience nonadiabatic relaxation and charge transfer processes to trigger the consequent photoreactions. In this sense, our simulation addresses the photoinduced water splitting processes in realistic systems.

Furthermore, we investigate the role of interfacial water configurations in this photocatalysis reaction. Different from the water adsorption on some metal oxide surfaces,[39,40] the 2D polymeric structure of g-C_3N_4 contains intrinsic vacancies which serve as new adsorption sites and catalytic centers. There are two major adsorption forms[22] of water molecules on the intrinsic vacancy in g-C_3N_4 nanosheet: Λ-type and Γ-type

https://doi.org/10.1021/acs.nanolett.1c01187
Nano Lett. 2021, 21, 6449−6455

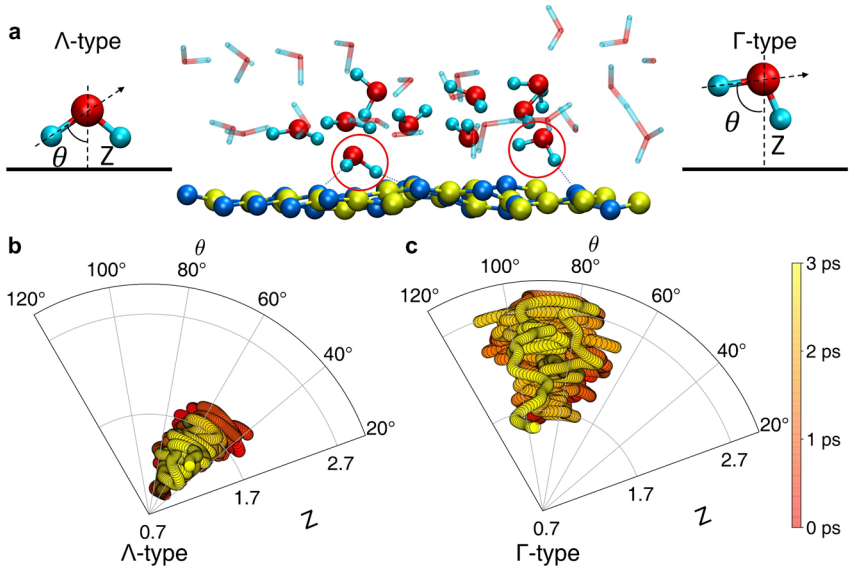

Figure 4. (a) Two typical configurations of interfacial water molecules (Λ- and Γ-type) on g-C_3N_4. Distributions of tilt angle (θ) and height (Z) for Λ- and Γ-type water molecules within a 3 ps MD trajectory are shown in parts b and c. The buckled g-C_3N_4 is considered as a planar sheet, and its position is calculated from the average position of all atoms in the sheet.

shown in Figure 4a, respectively. To give a quantitative description of the adsorption configuration, the tilt angle (θ) is defined as the angle between the O-H bond of water molecule and the normal direction of g-C_3N_4 surface, and the molecule height (Z) is the vertical distance of oxygen atom from the sheet.

We track the changes of tilt angle (θ) and height (Z) for Λ- and Γ-type molecules within the adiabatic 3 ps MD trajectory right before laser stimulation, in Figure 4, parts b and c. After the initiation of light excitation, the Λ-type molecule evolves into the splitting state under the influence of photocatalytic g-C_3N_4 (Figure 3a), while the Γ-type molecule remains intact throughout the whole excitation process (Figure S8). In comparison to the Γ-type, the lower height and smaller tilt angle of the Λ-type water strengthen the hydrogen bonding interactions between water and surface nitrogen, facilitating photoinduced charge transfer and subsequent photocatalytic reactions. Experimental studies have shown that introducing mesoporous or amorphous structure into g-C_3N_4 can significantly improve its photocatalytic efficiency,[12,13] which may be related to the increase of Λ-type water configurations.

The knowledge that the split hydrogen atoms are adsorbed on the active nitrogen site of g-C_3N_4 enables us to establish a molecular understanding for hydrogen gas formation. Although the H_2 formation has a low probability in straightforward molecular dynamics simulations, we can investigate the associated potential energy surfaces of H_2 formation near the reaction center using the climbing-image nudged elastic band (CI-NEB) method.

Potential energy profiles in Figure 5 show the diffusion barrier of H adsorbate from A site to B site at the reaction center, with a minimal barrier of 0.08 eV. It indicates a high diffusion rate at room temperature. However, diffusion from B to C site is a rate-limiting process, with a high energy barrier (2.3 eV) owing to the requisite of N−H bond breaking (see Figure S9). Thus, the hydrogen diffusion is confined on the nitrogen atoms at A and B sites. Two hydrogen atoms can desorb from A and B sites to form a H_2 molecule in Figure 5b. The transition state involves one hydrogen atom desorbing

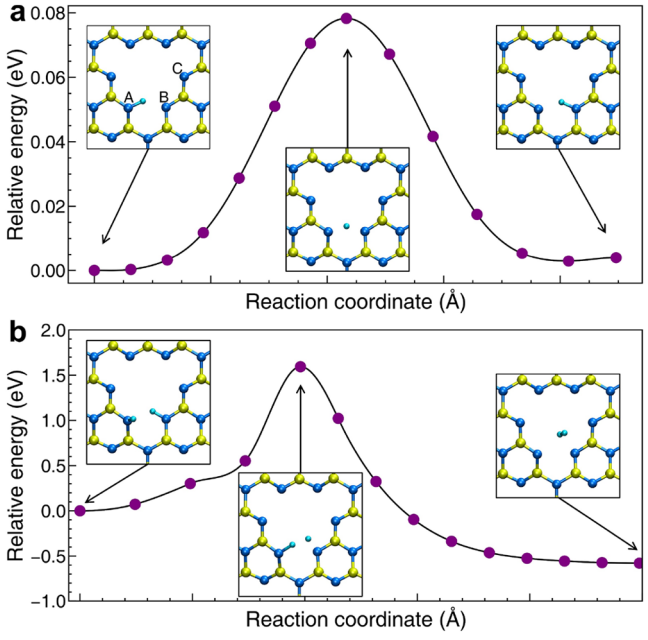

Figure 5. Potential energy profile for (a) hydrogen diffusion and (b) H_2 production near the reaction center. The nitrogen sites for hydrogen adsorption are labeled as A, B, and C sites in part a.

from the sheet and approaching the other H atom at A site. The activation barrier for H_2 formation is 1.5 eV, comparable to the typical barrier for the Volmer−Tafel reaction on the 1T-MoS_2 nanosheets.[41] Therefore, the H_2 gas formation is attributed to the following processes: Once a hydrogen atom jumps from A to B site, another water molecule splits and the split hydrogen atom fills the empty A site; then the two hydrogen atoms will recombine to form a H_2 molecule. Furthermore, the nearby coexistence of two activated hydrogen atoms, which have excess energy from incident photons, may also encounter lower activation barriers than that in the static calculations. On the other hand, the remnant OH radicals in

https://doi.org/10.1021/acs.nanolett.1c01187
Nano Lett. 2021, 21, 6449−6455

the aqueous solution may be accumulated to form hydrogen peroxide (H_2O_2) or oxygen gas in a longer time scale.[11]

In conclusion, we report quantum nonadiabatic dynamics simulations of photocatalytic water splitting process on g-C_3N_4 sheet, where the quantum motions of charge carriers (electron/hole) in the excited state are captured within the rt-TDDFT MD framework. We suggest a three-step reaction mechanism which includes photoexcitation, oxidation transfer and reduction transfer stages, corresponding to the photogeneration of charge carriers in g-C_3N_4, the hole transfer process from g-C_3N_4 to water, and bond breaking/re-forming reactions at the interface, respectively. In addition, water molecule that forms two hydrogen bonds with nitrogen atoms favors the photolysis reaction under light irritation. We also identify that hydrogen gas can be naturally formed via Tafel-like reaction near the reaction center, where two split hydrogen atoms are recombined. Hydrogen peroxide can be formed by remnant hydroxyl radicals. Thus, the whole mechanism of photocatalytic hydrogen evolution is complete in such an atomistic pathway: photoexcited electron transitions → transport of photocarriers → hole-driven hydrogen transfer → hydrogen gas evolution. Our studies provide a comprehensive understanding on how the photoexcited charge transfer drives water splitting reactions on a representative polymeric semiconductor g-C_3N_4, which is vital for revealing the nature of photocatalysis and improving further the efficiency of g-C_3N_4-based photocatalytic materials.

■ ASSOCIATED CONTENT

Supporting Information

The Supporting Information is available free of charge at https://pubs.acs.org/doi/10.1021/acs.nanolett.1c01187.

Detailed methods, analysis of electronic structure, quantum dynamics, and benchmark calculations (PDF)

■ AUTHOR INFORMATION

Corresponding Authors

Cui Zhang − *Beijing National Laboratory for Condensed Matter Physics and Institute of Physics, Chinese Academy of Sciences, Beijing 100190, People's Republic of China; Songshan Lake Materials Laboratory, Dongguan, Guangdong 523808, People's Republic of China*; Email: cuizhang@iphy.ac.cn

Sheng Meng − *Beijing National Laboratory for Condensed Matter Physics and Institute of Physics, Chinese Academy of Sciences, Beijing 100190, People's Republic of China; Songshan Lake Materials Laboratory, Dongguan, Guangdong 523808, People's Republic of China; School of Physical Sciences, University of Chinese Academy of Sciences, Beijing 100049, People's Republic of China*; orcid.org/0000-0002-1553-1432; Email: smeng@iphy.ac.cn

Enge Wang − *Beijing National Laboratory for Condensed Matter Physics and Institute of Physics, Chinese Academy of Sciences, Beijing 100190, People's Republic of China; Songshan Lake Materials Laboratory, Dongguan, Guangdong 523808, People's Republic of China; International Center for Quantum Materials and School of Physics, Peking University, Beijing 100871, People's Republic of China; School of Physics, Liaoning University, Shenyang 110136, People's Republic of China*; Email: egwang@pku.edu.cn

Authors

Peiwei You − *Beijing National Laboratory for Condensed Matter Physics and Institute of Physics, Chinese Academy of Sciences, Beijing 100190, People's Republic of China; School of Physical Sciences, University of Chinese Academy of Sciences, Beijing 100049, People's Republic of China*; orcid.org/0000-0003-1606-4810

Chao Lian − *Beijing National Laboratory for Condensed Matter Physics and Institute of Physics, Chinese Academy of Sciences, Beijing 100190, People's Republic of China*

Daqiang Chen − *Beijing National Laboratory for Condensed Matter Physics and Institute of Physics, Chinese Academy of Sciences, Beijing 100190, People's Republic of China; School of Physical Sciences, University of Chinese Academy of Sciences, Beijing 100049, People's Republic of China*

Jiyu Xu − *Beijing National Laboratory for Condensed Matter Physics and Institute of Physics, Chinese Academy of Sciences, Beijing 100190, People's Republic of China; School of Physical Sciences, University of Chinese Academy of Sciences, Beijing 100049, People's Republic of China*; orcid.org/0000-0002-2628-5492

Complete contact information is available at: https://pubs.acs.org/10.1021/acs.nanolett.1c01187

Notes

The authors declare no competing financial interest.

■ ACKNOWLEDGMENTS

We acknowledge financial support from National Natural Science Foundation of China (NSFC Grant Nos. 12025407, 11974400, 11474328, and 91850120), the Ministry of Science and Technology of the People's Republic of China (MOST Grant No. 2016YFA0300902), and the "Strategic Priority Research Program B" of the CAS (No. XDB330301).

■ REFERENCES

(1) Wang, X.; Maeda, K.; Thomas, A.; Takanabe, K.; Xin, G.; Carlsson, J. M.; Domen, K.; Antonietti, M. A metal-free polymeric photocatalyst for hydrogen production from water under visible light. *Nat. Mater.* **2009**, *8* (1), 76−80.

(2) Wang, X.; Maeda, K.; Chen, X.; Takanabe, K.; Domen, K.; Hou, Y.; Fu, X.; Antonietti, M. Polymer Semiconductors for Artificial Photosynthesis: Hydrogen Evolution by Mesoporous Graphitic Carbon Nitride with Visible Light. *J. Am. Chem. Soc.* **2009**, *131* (5), 1680−1681.

(3) Maeda, K.; Wang, X.; Nishihara, Y.; Lu, D.; Antonietti, M.; Domen, K. Photocatalytic Activities of Graphitic Carbon Nitride Powder for Water Reduction and Oxidation under Visible Light. *J. Phys. Chem. C* **2009**, *113* (12), 4940−4947.

(4) Ong, W. J.; Tan, L. L.; Ng, Y. H.; Yong, S. T.; Chai, S. P. Graphitic Carbon Nitride (g-C_3N_4)-Based Photocatalysts for Artificial Photosynthesis and Environmental Remediation: Are We a Step Closer To Achieving Sustainability? *Chem. Rev.* **2016**, *116* (12), 7159−329.

(5) Dai, Y.; Li, C.; Shen, Y.; Lim, T.; Xu, J.; Li, Y.; Niemantsverdriet, H.; Besenbacher, F.; Lock, N.; Su, R. Light-tuned selective photosynthesis of azo- and azoxy-aromatics using graphitic C_3N_4. *Nat. Commun.* **2018**, *9* (1), 60.

(6) Feng, J.; Gao, H.; Zheng, L.; Chen, Z.; Zeng, S.; Jiang, C.; Dong, H.; Liu, L.; Zhang, S.; Zhang, X. A Mn-N_3 single-atom catalyst embedded in graphitic carbon nitride for efficient CO_2 electroreduction. *Nat. Commun.* **2020**, *11* (1), 4341.

(7) Shiraishi, Y.; Ueda, Y.; Soramoto, A.; Hinokuma, S.; Hirai, T. Photocatalytic hydrogen peroxide splitting on metal-free powders

assisted by phosphoric acid as a stabilizer. *Nat. Commun.* **2020**, *11* (1), 3386.
(8) Li, X.; Bi, W.; Zhang, L.; Tao, S.; Chu, W.; Zhang, Q.; Luo, Y.; Wu, C.; Xie, Y. Single-Atom Pt as Co-Catalyst for Enhanced Photocatalytic H_2 Evolution. *Adv. Mater.* **2016**, *28* (12), 2427−31.
(9) Zhang, J.; Sun, J.; Maeda, K.; Domen, K.; Liu, P.; Antonietti, M.; Fu, X.; Wang, X. Sulfur-mediated synthesis of carbon nitride: Band-gap engineering and improved functions for photocatalysis. *Energy Environ. Sci.* **2011**, *4* (3), 675−678.
(10) Liu, G.; Niu, P.; Sun, C.; Smith, S. C.; Chen, Z.; Lu, G. Q.; Cheng, H.-M. Unique Electronic Structure Induced High Photoreactivity of Sulfur-Doped Graphitic C_3N_4. *J. Am. Chem. Soc.* **2010**, *132* (33), 11642−11648.
(11) Liu, J.; Liu, Y.; Liu, N.; Han, Y.; Zhang, X.; Huang, H.; Lifshitz, Y.; Lee, S.-T.; Zhong, J.; Kang, Z. Metal-free efficient photocatalyst for stable visible water splitting via a two-electron pathway. *Science* **2015**, *347*, 970−974.
(12) He, F.; Chen, G.; Zhou, Y.; Yu, Y.; Zheng, Y.; Hao, S. The facile synthesis of mesoporous g-C_3N_4 with highly enhanced photocatalytic H_2 evolution performance. *Chem. Commun.* **2015**, *51* (90), 16244−6.
(13) Kang, Y.; Yang, Y.; Yin, L. C.; Kang, X.; Liu, G.; Cheng, H. M. An Amorphous Carbon Nitride Photocatalyst with Greatly Extended Visible-Light-Responsive Range for Photocatalytic Hydrogen Generation. *Adv. Mater.* **2015**, *27* (31), 4572−7.
(14) Zhang, J.; Zhang, M.; Zhang, G.; Wang, X. Synthesis of Carbon Nitride Semiconductors in Sulfur Flux for Water Photoredox Catalysis. *ACS Catal.* **2012**, *2* (6), 940−948.
(15) Zhu, M.; Kim, S.; Mao, L.; Fujitsuka, M.; Zhang, J.; Wang, X.; Majima, T. Metal-Free Photocatalyst for H_2 Evolution in Visible to Near-Infrared Region: Black Phosphorus/Graphitic Carbon Nitride. *J. Am. Chem. Soc.* **2017**, *139* (37), 13234−13242.
(16) Qian, X.; Ding, J.; Zhang, J.; Zhang, Y.; Wang, Y.; Kan, E.; Wang, X.; Zhu, J. Ultrathin molybdenum disulfide/carbon nitride nanosheets with abundant active sites for enhanced hydrogen evolution. *Nanoscale* **2018**, *10* (4), 1766−1773.
(17) Hou, Y.; Laursen, A. B.; Zhang, J.; Zhang, G.; Zhu, Y.; Wang, X.; Dahl, S.; Chorkendorff, I. Layered nanojunctions for hydrogen-evolution catalysis. *Angew. Chem., Int. Ed.* **2013**, *52* (13), 3621−5.
(18) Du, A.; Sanvito, S.; Li, Z.; Wang, D.; Jiao, Y.; Liao, T.; Sun, Q.; Ng, Y. H.; Zhu, Z.; Amal, R.; Smith, S. C. Hybrid graphene and graphitic carbon nitride nanocomposite: gap opening, electron-hole puddle, interfacial charge transfer, and enhanced visible light response. *J. Am. Chem. Soc.* **2012**, *134* (9), 4393−7.
(19) Li, X.; Dai, Y.; Ma, Y.; Han, S.; Huang, B. Graphene/g-C_3N_4 bilayer: considerable band gap opening and effective band structure engineering. *Phys. Chem. Chem. Phys.* **2014**, *16* (9), 4230−5.
(20) Zhang, L.; Long, R.; Zhang, Y.; Duan, D.; Xiong, Y.; Zhang, Y.; Bi, Y. Direct Observation for Dynamic Bond Evolution in Single-Atom Pt/C_3N_4 Catalysts. *Angew. Chem., Int. Ed.* **2020**, *59* (15), 6224−6229.
(21) Wu, H. Z.; Liu, L. M.; Zhao, S. J. The effect of water on the structural, electronic and photocatalytic properties of graphitic carbon nitride. *Phys. Chem. Chem. Phys.* **2014**, *16* (7), 3299−304.
(22) Wu, H.-Z.; Liu, L.-M.; Zhao, S.-J. The role of the defect on the adsorption and dissociation of water on graphitic carbon nitride. *Appl. Surf. Sci.* **2015**, *358*, 363−369.
(23) Aspera, S. M.; David, M.; Kasai, H. First-Principles Study of the Adsorption of Water on Tri-s-triazine-based Graphitic Carbon Nitride. *Jpn. J. Appl. Phys.* **2010**, *49* (11), 115703.
(24) Pham, T. A.; Ping, Y.; Galli, G. Modelling heterogeneous interfaces for solar water splitting. *Nat. Mater.* **2017**, *16* (4), 401−408.
(25) Akimov, A. V.; Muckerman, J. T.; Prezhdo, O. V. Nonadiabatic dynamics of positive charge during photocatalytic water splitting on GaN(10−10) surface: charge localization governs splitting efficiency. *J. Am. Chem. Soc.* **2013**, *135* (23), 8682−91.
(26) Akimov, A. V.; Neukirch, A. J.; Prezhdo, O. V. Theoretical Insights into Photoinduced Charge Transfer and Catalysis at Oxide Interfaces. *Chem. Rev.* **2013**, *113* (6), 4496−4565.
(27) You, P.; Chen, D.; Lian, C.; Zhang, C.; Meng, S. First-principles dynamics of photoexcited molecules and materials towards a quantum description. *Wiley Interdiscip. Rev.: Comput. Mol. Sci.* **2021**, *11*, No. e1492.
(28) Yan, L.; Xu, J.; Wang, F.; Meng, S. Plasmon-Induced Ultrafast Hydrogen Production in Liquid Water. *J. Phys. Chem. Lett.* **2018**, *9* (1), 63−69.
(29) Yan, L.; Meng, S. Atomistic insights into plasmon induced water splitting. *Sci. China: Phys., Mech. Astron.* **2017**, *60* (2), 027032.
(30) Yan, L.; Wang, F.; Meng, S. Quantum Mode Selectivity of Plasmon-Induced Water Splitting on Gold Nanoparticles. *ACS Nano* **2016**, *10* (5), 5452−8.
(31) Alonso, J. L.; Andrade, X.; Echenique, P.; Falceto, F.; Prada-Gracia, D.; Rubio, A. Efficient formalism for large-scale ab initio molecular dynamics based on time-dependent density functional theory. *Phys. Rev. Lett.* **2008**, *101* (9), 096403.
(32) Miyamoto, Y.; Zhang, H.; Cheng, X.; Rubio, A. Modeling of laser-pulse induced water decomposition on two-dimensional materials by simulations based on time-dependent density functional theory. *Phys. Rev. B: Condens. Matter Mater. Phys.* **2017**, *96* (11), 115451.
(33) Miyamoto, Y.; Zhang, H.; Cheng, X.; Rubio, A. Ab initio simulation of laser-induced water decomposition close to carbon nanotubes. *Phys. Rev. B: Condens. Matter Mater. Phys.* **2019**, *99* (16), 165424.
(34) Ullah, N.; Chen, S.; Zhao, Y.; Zhang, R. Photoinduced Water-Heptazine Electron-Driven Proton Transfer: Perspective for Water Splitting with g-C_3N_4. *J. Phys. Chem. Lett.* **2019**, *10* (15), 4310−4316.
(35) Shin, H. J.; Jung, J.; Motobayashi, K.; Yanagisawa, S.; Morikawa, Y.; Kim, Y.; Kawai, M. State-selective dissociation of a single water molecule on an ultrathin MgO film. *Nat. Mater.* **2010**, *9* (5), 442−7.
(36) Zhang, M.; de Respinis, M.; Frei, H. Time-resolved observations of water oxidation intermediates on a cobalt oxide nanoparticle catalyst. *Nat. Chem.* **2014**, *6* (4), 362−7.
(37) Wang, L. W. Natural Orbital Branching Scheme for Time-Dependent Density Functional Theory Nonadiabatic Simulations. *J. Phys. Chem. A* **2020**, *124* (43), 9075−9087.
(38) Bang, J.; Sun, Y. Y.; Liu, X. Q.; Gao, F.; Zhang, S. B. Carrier-Multiplication-Induced Structural Change during Ultrafast Carrier Relaxation and Nonthermal Phase Transition in Semiconductors. *Phys. Rev. Lett.* **2016**, *117* (12), 126402.
(39) Wendt, S.; Matthiesen, J.; Schaub, R.; Vestergaard, E. K.; Laegsgaard, E.; Besenbacher, F.; Hammer, B. Formation and splitting of paired hydroxyl groups on reduced TiO_2(110). *Phys. Rev. Lett.* **2006**, *96* (6), 066107.
(40) Schaub, R.; Thostrup, P.; Lopez, N.; Laegsgaard, E.; Stensgaard, I.; Norskov, J. K.; Besenbacher, F. Oxygen vacancies as active sites for water dissociation on rutile TiO_2(110). *Phys. Rev. Lett.* **2001**, *87* (26), 266104.
(41) Tang, Q.; Jiang, D.-e. Mechanism of Hydrogen Evolution Reaction on 1T-MoS_2 from First Principles. *ACS Catal.* **2016**, *6* (8), 4953−4961.

https://doi.org/10.1021/acs.nanolett.1c01187
Nano Lett. 2021, 21, 6449−6455